DOI: 10.1002/ejic.201100640

Octahedral Molybdenum(0) Monodinitrogen Complexes Facially Coordinated by the Tripodal Ligand 1,1,1-Tris(diphenylphosphanylmethyl)ethane – Influence of Diphosphane Coligands on the Activation of N_2

Jan Krahmer,[a] Henning Broda,[a] Christian Näther,[a] Gerhard Peters,[a] Wulf Thimm,[a] and Felix Tuczek*[a]

Keywords: Molybdenum / Nitrogen / P ligands / Nitrogen fixation / Tripodal ligands

The synthesis and physicochemical properties of the new molybdenum dinitrogen complexes [Mo(N_2)(tdppme)(dmpm)] (**2**) and [Mo(N_2)(tdppme)(dppm)] (**3**) are reported. Complexes **2** and **3** are facially coordinated by the tripodal ligand 1,1,1-tris(diphenylphosphanylmethyl)ethane (tdppme) and contain the bidentate coligands bis(dimethylphosphanyl)methane (dmpm) and bis(diphenylphosphanyl)methane (dppm), respectively. They are accessible by amalgam reduction of the Mo^{III} precursor [$MoBr_3$(tdppme)] (**1**) under nitrogen in the presence of dppm and dmpm, respectively. Protonation of **2** with trifluoromethanesulfonic acid (triflic acid, HOTf) leads to the NNH_2 complex [Mo(NNH_2)(tdppme)(dmpm)]$(OTf)_2$ (**4**) with retention of the pentaphosphane coordination. The structural, electronic and vibrational properties of **2**, **3** and **4** have been investigated by NMR, IR and Raman spectroscopy coupled with DFT calculations. The crystal structure of **2** has been determined and is discussed in relation to the calculated structures of **2** and **3**. The results of the investigations are compared with those obtained earlier for the pentaphosphane complexes [Mo(N_2)(dpepp)(dppm)] and [Mo(NNH_2)(dpepp)(dppm)]$(OTf)_2$ [dpepp = bis(diphenylphosphanylethyl)phenylphosphane].

Introduction

One of the fundamental reactions of nature is the fixation of molecular nitrogen as ammonia in plants and bacteria. This reaction proceeds at a unique iron/molybdenum/sulfur cluster, the FeMoco, which is located in the MoFe protein of the enzyme nitrogenase.[1–6] There have been numerous attempts to reproduce biological nitrogen fixation by small-molecule model systems.[7,8] Two well-established mechanistic schemes in this regard are represented by the Schrock and Chatt cycles, which are based on molybdenum triamidoamine and phosphane complexes, respectively. In both cases the Mo–dinitrogen complex can be converted to complexes of NNH_x and NH_x species by a series of protonation and reduction steps, which ultimately lead to ammonia.[9,10] For the Schrock cycle a catalytic conversion of N_2 to ammonia has been demonstrated in 6–8 cycles with an overall yield of 65%.[11–13] It is a challenge to achieve a catalytic action with a comparable efficiency for Chatt-type molybdenum–phosphane complexes.[14,15] Recently, a dimolybdenum–dinitrogen complex bearing two PNP pincer ligands [PNP = 2,6-bis(di-*tert*-butylphosphanylmethyl)pyridine] was found to work as an effective catalyst for the formation of ammonia from dinitrogen, with 12 equiv. of ammonia being produced per molybdenum atom of the catalyst.[16] Detailed insight into the mechanism of this reaction is, however, difficult due to the presence of five dinitrogen ligands (four terminal, one bridging) in the dinuclear Mo^0 complex.[17]

Our group has been involved in a detailed experimental and theoretical investigation of the Chatt cycle for a number of years.[18] One of the major mechanistic problems of this cycle is connected with the exchange of one of the two dinitrogen ligands of the parent Mo^0 bis(dinitrogen) complex by the conjugate base of the acid employed for the protonation reaction. In particular, the presence of anionic coligands leads to disproportionation reactions at the Mo^I stage and renders the formation of the pivotal Mo^0 bis(dinitrogen) complex difficult. One of the synthetic strategies to cope with this problem involves the design of ligands occupying the *trans* position of the dinitrogen ligand in the Mo^0 complex. This concept has already been pursued by George and co-workers through the synthesis of molybdenum dinitrogen complexes supported by linear tridentate phosphane ligands of the type Ph_2P–$(CH_2)_2$–E–$(CH_2)_2$–PPh_2 (PEP).[19,20] In the spirit of this approach, Mo–N_2–PNHP (E = NH), –PNMeP (E = NMe), –PSP (E = S) and –POP (E = O) complexes have been prepared and characterized.[21] The majority of data, however, have been obtained from complexes with the dpepp ligand (E = PPh).[22] These systems have been synthesized with bidentate phosphane coligands such as dppe or dppm. We have augmented this series with the synthesis and characterization of

[a] Institut für Anorganische Chemie, Christian-Albrechts-Universität zu Kiel
Max-Eyth-Str. 2, 24118 Kiel, Germany
E-mail: ftuczek@ac.uni-kiel.de

Supporting information for this article is available on the WWW under http://dx.doi.org/10.1002/ejic.201100640.

[Mo(N_2)(dpepp)(depe)] and [Mo(N_2)(dpepp)(1,2-dppp)] [1,2-dppp = $Ph_2PCH(CH_3)CH_2PPh_2$].[23] As first demonstrated by George et al. and supported by our own experiments, [Mo(N_2)(dpepp)(dppm)] can be protonated by triflic acid with retention of the pentaphosphane ligation, thus making this system a candidate for the catalytic conversion of N_2 to ammonia on the basis of Mo–phosphane systems. A corresponding mechanistic cycle has been evaluated by DFT.[24] The stoichiometric production of ammonia by protonation of [Mo(N_2)(dpepp)(diphosphane)] complexes has extensively been investigated by George et al.[25]

A fundamental problem of Mo(dpepp)(diphosphane)–dinitrogen complexes is the existence of two isomers. Specifically, the central P donor of the dpepp ligand can coordinate in the *trans* or *cis* position to the dinitrogen ligand, which leads to the *ortho*- and *iso* forms of the complexes, respectively.[23] Both isomers can be distinguished by the degree of activation imparted to the dinitrogen ligand. In order to avoid this complication, we decided to employ tripodal ligands, which can only bind in one configuration. So far, this strategy has not been applied to molybdenum dinitrogen complexes, and it is the purpose of this paper to fill this gap. To this end, the synthesis and characterization of [Mo(N_2)(tdppme)(dmpm)] (**2**) and [Mo(N_2)(tdppme)(dppm)] (**3**) are reported. Both complexes can be prepared by Na_x/Hg reduction of the Mo^{III} compound [$MoBr_3$(tdppme)] (**1**) under N_2. A new synthesis for this important precursor is also presented. The structural, electronic and vibrational properties of **2** and **3** are determined, and their reactivities towards acids are evaluated. The results are compared with those obtained earlier in the investigation of [Mo(N_2)(dpepp)(diphosphane)] systems, and the implications on the reduction and protonation of N_2 in Chatt-type systems are discussed.

Results and Discussion

[$MoBr_3$(tdppme)] (1)

In order to obtain dinitrogen complexes supported by the tripodal ligand 1,1,1-tris(diphenylphosphanylmethyl) ethane (tdppme), we started from the molybdenum(III) precursor [$MoBr_3(THF)_3$]. The published synthesis of **1** by bromination of [$Mo(CO)_3$(tdppme)][29] gave us unsatisfactory results. Instead, by heating a mixture of tdppme and [$MoBr_3(THF)_3$] in toluene to reflux, [$MoBr_3$(tdppme)] (**1**) was obtained in high yield and purity.

[Mo(N_2)(tdppme)(dmpm)] (2) and [Mo($^{15}N_2$)(tdppme)(dmpm)] (2a)

By reduction of **1** with sodium amalgam in THF under N_2 in the presence of bis(dimethylphosphanyl)methane (dmpm), the dinitrogen complex [Mo(N_2)(tdppme)(dmpm)] (**2**) was formed. Single crystals suitable for an X-ray structure determination were grown by recrystallization from a toluene/*n*-hexane mixture. Orthorhombic **2** crystallizes in the noncentrosymmetric space group $Pna2_1$ with $Z = 4$ molecules in the unit cell (Table 1). The tripodal ligand tdppme coordinates facially to the molybdenum centre, and the three remaining coordination sites are occupied by one bidentate dmpm ligand and one molecule of dinitrogen (Figure 1). The coordination sphere of **2** is octahedral with a trigonal distortion. The Mo–P bond lengths of the phosphane ligands vary between 2.3986(16) and 2.4454(16) Å (Table 2) and thus are slightly shorter than those of [Mo(N_2)(dpepp)(dppm)], which lie between 2.418(2) and 2.497(2) Å (Table 3).[22] The Mo–N bond length of **2** is 2.066(6) Å, which is slightly longer than that in [Mo(N_2)(dpepp)(dppm)] [2.025(6) Å]. On the other hand, the N–N bond length of **2** [1.069(8) Å] is somewhat shorter than that in [Mo(N_2)(dpepp)(dppm)] [1.119(8) Å].[22]

Table 1. Summary of crystallographic data for **2**.

Formula	$C_{46}H_{53}MoN_2P_5$
M_w [g mol^{-1}]	884.69
Crystal system	orthorhombic
Space group	$Pna2_1$
a [Å]	21.763(3)
b [Å]	13.972(2)
c [Å]	14.253(2)
V [Å^3]	4333.8(7)
T [K]	170
Z	4
$D_{calcd.}$ [g cm^{-3}]	1.356
μ [mm^{-1}]	0.522
θ_{max} [°]	25.00
Measured reflections	25417
Unique reflections	6746
R_{int}	0.0981
Reflections [$F_0 > 4s(F_0)$]	5561
Parameters	488
R_1 [$F_0 > 4s(F_0)$]	0.0482
wR_2 [all data]	0.1167
GOF	1.003
Δr_{max}, Δr_{min} [e Å^{-3}]	0.576, –0.839

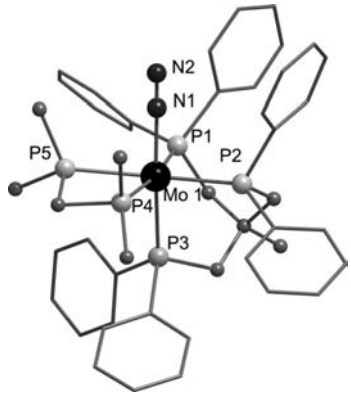

Figure 1. Molecular structure of [Mo(N_2)(tdppme)(dmpm)] (**2**) (hydrogen atoms omitted, phenyl groups drawn as wireframes).

The P–Mo–P angles of **2** lie between 82.30(5) and 86.00(6)° and thus are significantly smaller than 90°, which indicates a trigonal elongation of the octahedral coordination sphere. Their values closely agree with the P–Mo–P angles in [Mo(tdppme)($CO)_3$].[30] The coordinated tripodal

Table 2. Selected bond lengths [Å] and angles [°] for [Mo(N_2)(tdppme)(dmpm)] (**2**).

Bond lengths		Angles	
Mo(1)–N(1)	2.066(6)	N(1)–Mo(1)–P(2)	91.54(17)
Mo(1)–P(2)	2.3986(16)	N(1)–Mo(1)–P(1)	93.04(15)
Mo(1)–P(1)	2.4363(15)	P(2)–Mo(1)–P(1)	82.30(5)
Mo(1)–P(3)	2.4454(16)	N(1)–Mo(1)–P(3)	177.37(17)
Mo(1)–P(4)	2.5033(16)	P(2)–Mo(1)–P(3)	86.00(6)
Mo(1)–P(5)	2.5101(16)	P(1)–Mo(1)–P(3)	85.73(5)
N(1)–N(2)	1.069(8)	N(1)–Mo(1)–P(4)	84.32(15)
		P(2)–Mo(1)–P(4)	105.73(5)
		P(1)–Mo(1)–P(4)	171.57(6)
		P(3)–Mo(1)–P(4)	97.22(6)
		N(1)–Mo(1)–P(5)	85.16(17)
		P(2)–Mo(1)–P(5)	172.11(5)
		P(1)–Mo(1)–P(5)	104.99(6)
		P(3)–Mo(1)–P(5)	97.40(6)
		P(4)–Mo(1)–P(5)	66.86(6)
		N(2)–N(1)–Mo(1)	176.7(6)
		C(1)–C(2)–P(1)–Mo(1)	38.309(7)
		C(1)–C(3)–P(2)–Mo(1)	25.883(7)
		C(1)–C(4)–P(3)–Mo(1)	32.453(7)

ligand undergoes a helical distortion by rotation of the C(1)–$(CH_2)_3$ moiety around an axis connecting the Mo^0 centre and the central C atom C(1) of the ligand, in analogy to that for [Mo(tdppme)$(CO)_3$].[30] This distortion can be expressed by the dihedral C(1)–C–P–Mo angles of 38.309(7) for C(1)–C(2)–P(1)–Mo(1), 25.883(7) for C(1)–C(3)–P(2)–Mo(1) and 32.453(7)° for C(1)–C(4)–P(3)–Mo(1). The bite angle of the bidentate dmpm ligand is about 66.86(6)°, which matches the bite angle of dmpm in [MoBr(dpepp)(dmpm)] [66.7(1)°].[31] It is somewhat smaller as compared to that of the dppm [bis(diphenylphosphanyl)-methane] ligand in [Mo(N_2)(dpepp)(dppm)], which exhibits a bite angle of 68.3(1)°, most likely because of steric reasons.[22]

On the basis of its crystal structure, **2** was investigated by DFT. As evident from Table 3, the structural parameters derived from geometry optimization match those derived from the crystal structure fairly well. Mo–N and Mo–P distances are about 0.1 Å too large, which has been observed before in this type of calculation.[22,23] The geometry of **2** determined by single-crystal structure analysis and DFT geometry optimization is also preserved in solution, as inferred from NMR spectroscopy. The ^{31}P NMR spectrum of [Mo(N_2)(tdppme)(dmpm)] exhibits an AA′XX′B structure (Figure S1). Because of an overlap of the signals, however, it was not possible to determine the coupling constants. The multiplet at 39.90–39.11 ppm is assigned to the AA′ atoms P_c and P_d, and the multiplet at 40.48–40.08 ppm is assigned to the phosphorus atom P_e (B) of the tripodal ligand. The corresponding shifts are comparable to those of the tripodal ligand in **3** (see below). The multiplet at –22.54 to –23.54 ppm belongs to the XX′ atoms P_a/P_b of the dmpm ligand. The negative shift of the diphos signal is compatible with the higher shielding of the phosphorus nuclei by the methyl groups of dmpm relative to that of the diphenylphosphane groups of the tripodal ligand. The assignment of the signals was supported by the ^1H-^{31}P HMBC spectrum (Figure S2). In particular, the coupling of the phenyl protons with the tripodal ligand P atoms, P_c, P_d and P_e, is observed. The coupling between the P atoms P_a and P_b of the dmpm ligand with its methyl protons is also visible.

Specific information with respect to the activation of N_2 in dinitrogen complexes can be obtained from vibrational spectroscopy.[32] Complex **2** exhibits a N–N stretch at 1980 cm^{-1} (Tables 4 and 5 and Figure 2). Therefore, the activation of the N_2 ligand is stronger than that in **3** (see below) and comparable to that in [Mo(N_2)(dpepp)(dppm)] (Table 4).[22] The stronger activation of **2** relative to that of **3** results from the electron-donating effect of the dimethylphosphanyl groups of the dmpm ligand in relation to the π-acidic diphenylphosphanyl groups of dppm. The higher activation of N_2 also renders **2** susceptible to protonation by strong acids such as triflic acid (see below), in contrast to **3**.

In order to obtain more detailed vibrational spectroscopic information about **2**, [Mo($^{15}N_2$)(tdppme)(dmpm)] (**2a**) was also prepared, by using $^{15}N_2$ instead of $^{14}N_2$ gas. In **2a**, the N–N stretch shifts to 1915 cm^{-1} (1980 cm^{-1} in **2**, Tables 4 and 5, Figure 2). In the far-IR region, some isotope sensitive signals are also found (Figure 3); in particular, one band at 497 shifting to 490 cm^{-1} and two bands at 486/475 shifting to 483/472 cm^{-1} are observed. These features can be assigned on the basis of DFT calculations (Table 5). Importantly, these calculations place the Mo–N–N bending vibrations at higher energy than the Mo–N stretch. The band at 497 cm^{-1} that exhibits a shift to 490 cm^{-1} is thus assigned to one of the Mo–N–N bending vibrations, and the two bands at 486 and 475 cm^{-1} that shift to 483 and 472 cm^{-1}, respectively, are assigned to the Mo–N stretch, distributed over two vibrations. These frequencies are comparable to those observed for [Mo(N_2)(dpepp)(dppm)].[22]

Table 3. Selected bond lengths [Å] and angles [°] for the crystal structure of [Mo(N_2)(tdppme)(dmpm)] (**2**) and the calculated structures of [Mo(N_2)(tdppme)(dmpm)] (**2**) and [Mo(N_2)(tdppme)(dppm)] (**3**), in comparison with those of [Mo(N_2)(dpepp)(dppm)].[22]

	2 (expt.)	**2** (calcd.)	**3** (calcd.)	[Mo(N_2)(dpepp)(dppm)] (expt.)
N_α–N_β	1.069(8)	1.1579	1.1589	1.119(8)
Mo–N_α	2.066(6)	1.9823	1.9770	2.025(6)
Mo–$P_{a,b,c,d,e}$	2.3986(16)–2.4454(16)	2.4972–2.5942	2.5274–2.6597	2.418(2)–2.497(2)
N_α–N_β–Mo	177.372(6)	177.242	179.157	179.2(6)
N_β–Mo–P_e	177.372(4)	175.500	169.742	167.0(2)
P_a–Mo–P_b	66.856(6)	69.123	67.583	68.3(1)
P_c–Mo–P_d	82.301(5)	83.901	86.119	97.9(1)

Table 4. Comparison of the measured IR and Raman (R) frequencies of [Mo(N_2)(tdppme)(dmpm)] (**2**), [Mo(N_2)(tdppme)-(dppm)] (**3**) and [Mo(N_2)(dpepp)(dmpm)].[22]

	2		**3**	[Mo(N_2)(dpepp)(dppm)]	
	^{14}N [cm^{-1}]	^{15}N [cm^{-1}]	^{14}N [cm^{-1}]	^{14}N [cm^{-1}]	^{15}N [cm^{-1}]
ν(N–N)	1980 (IR)	1915 (IR)	2035 (IR)	1979 (IR)	1914 (IR)
	1979 (R)	1914 (R)	2040 (R)	1984/2003 (R)	1918/1935 (R)
ν(Mo–N–N)	497 (IR)	490 (IR)		505/497 (IR)	503/493 (IR)
ν(Mo–N)	486/475 (IR)	483/472 (IR)		453 (IR)	448 (IR)
				454 (R)	449 (R)

Table 5. Comparison of calculated and measured IR and Raman frequencies of [Mo(N_2)(tdppme)(dmpm)] (**2**).

	^{14}N [cm^{-1}] (meas.)	^{15}N [cm^{-1}] (meas.)	^{14}N [cm^{-1}] (calcd.)	^{15}N [cm^{-1}] (calcd.)
ν(N–N)	1979 (IR)	1914 (IR)	1924	1859
	1980 (R)	1915 (R)		
ν(Mo–N–N)	497 (IR)	490 (IR)	512	500
ν(Mo–N)	486/475	483/472	461	449
	(IR)	(IR)		

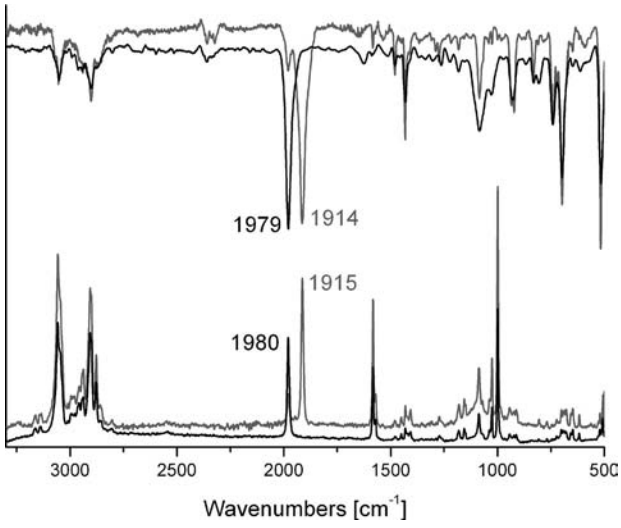

Figure 2. IR (top) and Raman (bottom) spectra of [Mo($^{14}N_2$)-(tdppme)(dmpm)] (**2**) (black) and [Mo($^{15}N_2$)(tdppme)(dmpm)] (**2a**) (grey).

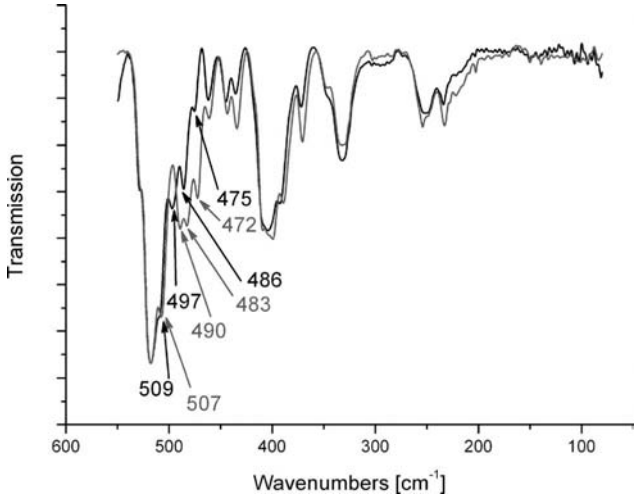

Figure 3. Far-IR spectrum of [Mo($^{14}N_2$)(tdppme)(dmpm)] (**2**) (black) and [Mo($^{15}N_2$)(tdppme)(dmpm)] (**2a**) (grey).

Complex **2a** was also investigated by ^{15}N NMR spectroscopy (Figure 4). The doublet at –25.61 ppm is attributed to the terminal nitrogen atom N_β ($^1J_{NN}$ = 5.90 Hz), and the multiplet at –33.09 to –33.63 ppm to the coordinated nitrogen atom N_α of the dinitrogen ligand. The splitting of the latter signal is induced by coupling with the molybdenum centre and the phosphane ligands. The N–N coupling constant and the shift for N_α approximately agree with the values found for [Mo($^{15}N_2$)(dpepp)(dppm)] [–30.355 to –30.712 (N_α, m), $^1J_{NN}$ = 5.7 Hz], whereas the signal of N_β is shifted to higher field relative to that of the latter system [–15.7 ppm (N_β)].[22]

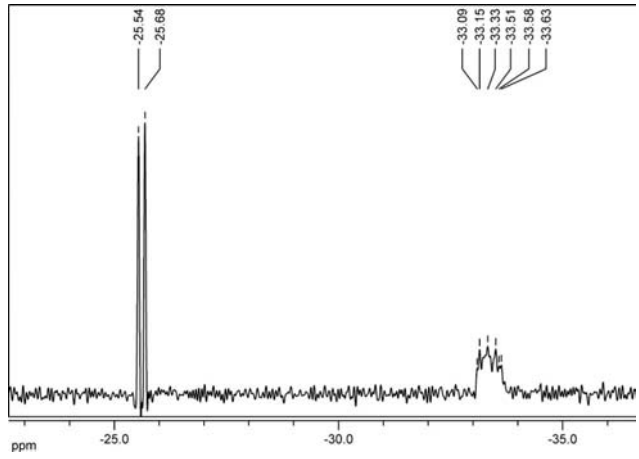

Figure 4. ^{15}N{^{1}H CPD} NMR spectrum of [Mo($^{15}N_2$)-(tdppme)(dmpm)] (**2a**) (CPD = composite pulse decoupling).

[Mo(N_2)(tdppme)(dppm)] (3)

The reduction of **1** with sodium amalgam in THF in the presence of dppm leads to the formation of the dinitrogen complex [Mo(N_2)(tdppme)(dppm)] (**3**). Single crystals of **3** suitable for an X-ray structure determination could not be

obtained. The structure of this complex was thus derived from a DFT geometry optimization. The topology of the complex is the same as that of **2**, with facial coordination of the tripodal ligand and bidentate coordination of the diphos ligand. A space-filling representation of the structure of **3** derived from this treatment is presented in Figure 5. The steric crowding around the metal centre imposed by the presence of five diphenylphosphane donors bearing ten phenyl rings is observed. Because of the presence of four phenyl groups above the equatorial plane, the apical N–N group is shielded fairly well.

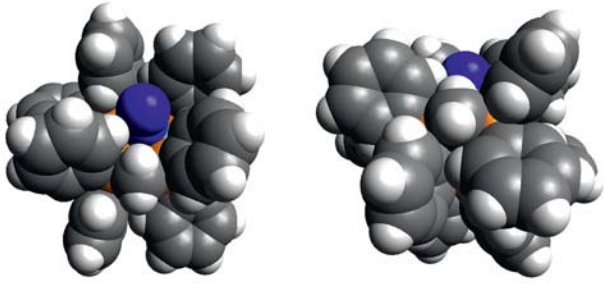

Figure 5. Space-filling structure of [Mo(dppm)(tdppme)N_2] (**3**) from the top (left) and from the side (right).

The ^{31}P NMR spectrum of **3** exhibits a typical AMM′XX′ pattern (Figure 6), which proves the presence of the geometry optimized structure in solution. The signal at 10.58 ppm is assigned to the XX′ phosphorus atoms of the dppm ligand, P_a and P_b. The signal at 43.92 ppm is associated with the equatorial MM′ atoms, P_c and P_d, of the tripodal ligand, and the signal at 33.32 ppm is attributed to its axial phosphane donor, P_e (A). The simulated spectrum was obtained by analysis of the M- and X-half-spectra according to the literature.[33] Each half-spectrum consists of ten lines, which, in turn, are split into doublets as a result of the interaction with P_e. The coupling constants between (P_c, P_d) and P_e are transmitted by the metal centre and the C_3 bridges of the tripodal ligand and have values of $^2J_{ed/ec}$ = –24.2 Hz. The same applies to $^2J_{cd}$, which has a somewhat larger value (–32.7 Hz). The *cis* coupling between the P_a and P_b donors of the diphos ligand, on the other hand, results from two interactions through the metal and the methylene bridge and has a value of $^2J_{ab}$ = –11.30 Hz. The remaining *cis* interactions are larger again, i.e. the coupling between P_e and the phosphorus atoms (P_a, P_b) of the dppm ligand has a magnitude of $^2J_{ea/eb}$ = –22.0 Hz, and the cis interactions between the dppm and tripodal ligands within the equatorial plane are $^2J_{ac/bd}$ = –27.78 Hz. As usual, *trans* interactions give rise to much larger splittings (91.13 Hz).

Complex **3** exhibits IR and Raman spectra with sharp vibrational features. The N–N stretch is located at 2035 cm^{-1} (Figure 7). The activation of the N_2 ligand in **3** is thus weaker than that in the dmpm complex **2**, which is due to the electron-withdrawing effect of the diphenylphosphanyl groups (vide supra). This conforms to our observation that we were not able protonate the N_2 ligand with triflic acid (see below). The far-IR spectrum of **3** (Figure S3) is qualitatively similar to that of **2** (Figure 3), exhibiting two clusters of bands located at about 400 cm^{-1} and between 450 and 500 cm^{-1}, respectively. Without further information from isotope substitution, however, the Mo–N stretch and Mo–N–N bending vibrations cannot be identified.

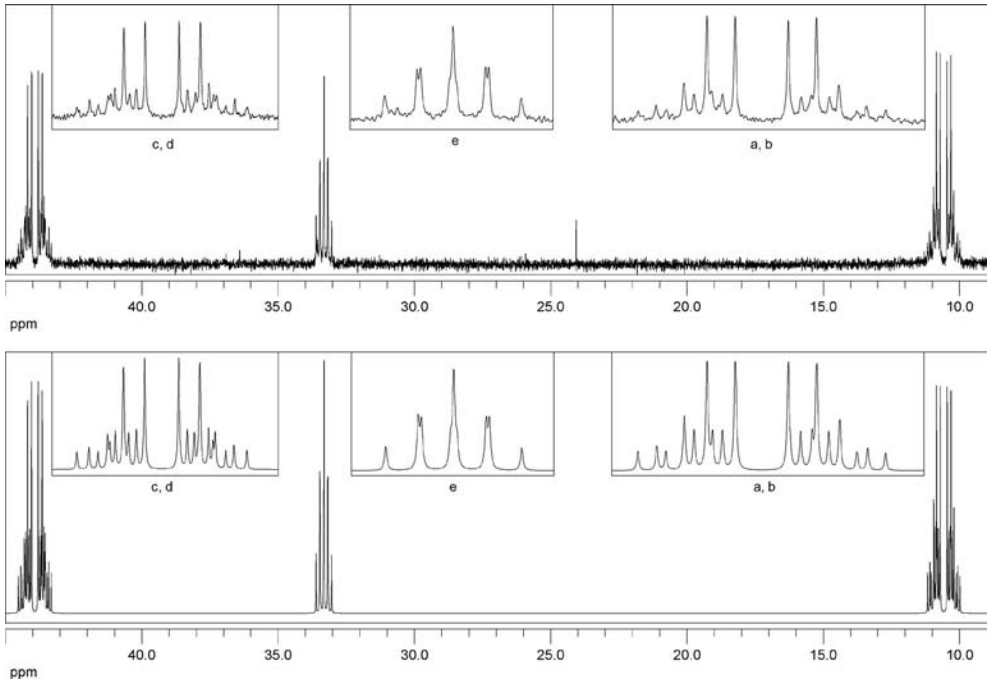

Figure 6. Measured (top) and simulated (bottom) $^{31}P\{^1H$ CPD$\}$ NMR spectrum of [Mo(N_2)(tdppme)(dppm)] (**3**).

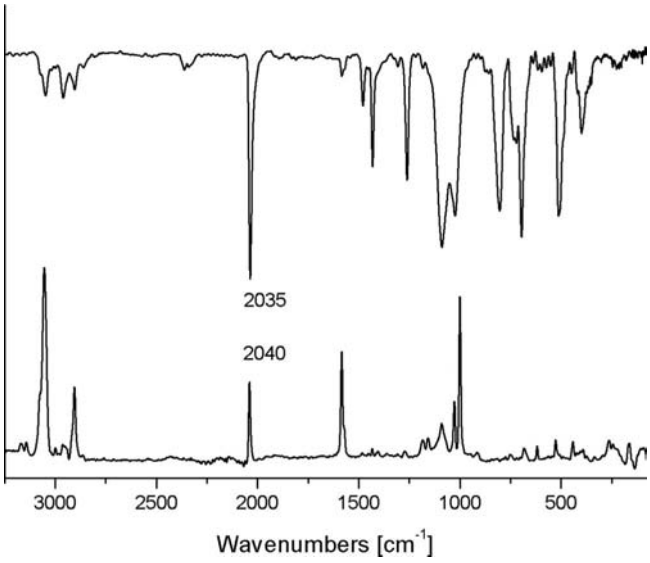

Figure 7. IR (top) and Raman (bottom) spectra of [Mo(N_2)(tdppme)(dppm)] (**3**).

[Mo(NNH_2)(tdppme)(dmpm)](OTf)$_2$ (4) and [Mo($^{15}N^{15}NH_2$)(tdppme)(dmpm)](OTf)$_2$ (4a)

As a result of moderate activation of the N_2 ligand, **2** could be protonated by using triflic acid, which led to the NNH_2 complex [Mo(NNH_2)(tdppme)(dmpm)](OTf)$_2$ (**4**). Similarly, the ^{15}N-substituted complex [Mo($^{15}N^{15}NH_2$)(tdppme)(dmpm)](OTf)$_2$ (**4a**) was obtained by protonation of the ^{15}N-isotopomer of **2**, **2a**.

The ^{31}P NMR spectrum of **4** again exhibits a typical AMM′XX′ pattern (Figure 8), which was analyzed in analogy to that of **3** (vide supra). The signal at –27.50 ppm belongs to the XX′ atoms, P_a and P_b, of the dmpm ligand; the signals at 21.50 and –4.40 ppm are assigned to the MM′ phosphorus atoms (P_c, P_d) and the axial A atom, P_e, of the tripodal ligand, respectively. With respect to the parent dinitrogen complex **2**, all ^{31}P resonances are shifted to higher field by 20–40 ppm. The simulated spectrum was obtained by analysis of the M- and X-half-spectra as described earlier. The coupling constants between the equatorial atoms P_c and P_d and the axial atom P_e of the tripodal ligand are $^2J_{ed/ec}$ = –29.44 Hz; the interaction of P_e with the phosphorus atoms (P_a, P_b) of the dppm ligand gives rise to coupling constants of a similar magnitude ($^2J_{ea/eb}$ = –31.03 Hz). Further *cis* interactions result in coupling constants of $^2J_{ab}$ = –9.55, $^2J_{ac/bd}$ = –24.85 and $^2J_{cd}$ = –18.75 Hz. At 83.15 Hz, the *trans* interactions have the usual large splitting. With increasing measuring time, two signals in the form of an AA′XX′ pattern evolve in the ^{31}P NMR spectrum of **4** at –23.35 and 24.82 ppm (marked by asterisks in Figure 8). These can be attributed to a decomposition product of **4**, probably arising from substitution of the axial atom, P_e, of the tripodal ligand by triflate.

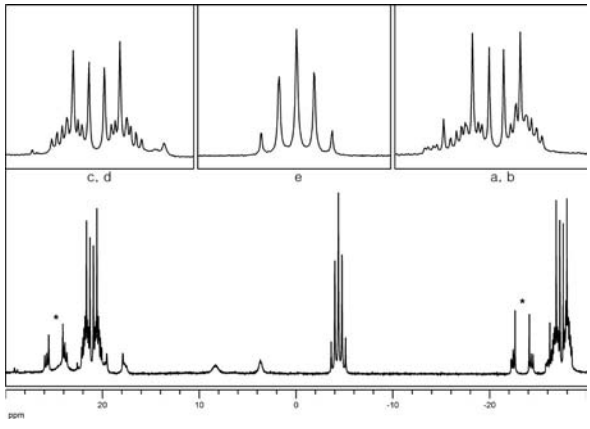

Figure 8. $^{31}P\{^1H$ CPD$\}$ NMR spectrum of [Mo(NNH_2)(tdppme)(dmpm)](OTf)$_2$ (**4**).

In the ^1H-^{15}N HMQC NMR spectrum (Figure 9) of **4a**, the coupling of the protons of the $^{15}N^{15}NH_2$ group (9.25 ppm) to the terminal $^{15}N_\beta$ atom (–217.84 ppm) can be observed. The shift for the protons was derived from the ^1H NMR spectrum, and the shift for the $^{15}N_\beta$ atom was derived from the cross-peak in the HMQC NMR spectrum. We were not able to determine the shifts for the $^{15}N_\alpha$ atom and the $^{15}N_\beta$ atom by regular ^{15}N NMR spectroscopy because of the limited solubility and decomposition of **4a** in solution (vide supra).

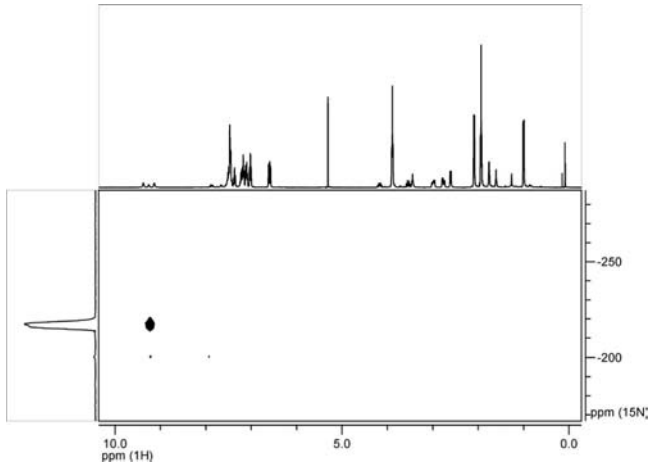

Figure 9. $^1H^{15}N$ HMQC NMR spectrum of [Mo($^{15}N^{15}NH_2$)(tdppme)(dmpm)](OTf)$_2$ (**4a**).

Important structural information can again be inferred from vibrational spectroscopy. The symmetric and antisymmetric NH_2 stretches of **4** are located at 3238 and 3301 cm^{-1} (Figure 10), which is at about the same frequency as that observed in [Mo(NNH_2)(dpepp)(dppm)] (Table 6).[22] In **4a**, the symmetric and antisymmetric NH_2 stretches are shifted to slightly lower energy (3230 and 3289 cm^{-1}, Figure 10). The N–N stretch of **4** is observed at 1410 cm^{-1}. However, the corresponding N–N stretch of **4a** is masked by the intense absorption of triflate. Again, these vibrational frequencies agree with results from DFT (Table 6). In particular, these calculations predict the symmetric NH_2 stretching vibration to be at lower frequency than the antisymmetric one.

Table 6. Comparison of calculated and measured IR and Raman frequencies of $[Mo(NNH_2)(tdppme)(dmpm)](OTf)_2$ (**4**) with those of $[Mo(NNH_2)(dpepp)(dppm)](OTf)_2$.[22]

	$[Mo(NNH_2)(tdppme)(dmpm)](OTf)_2$				$[Mo(NNH_2)(dpepp)(dppm)](OTf)_2$
	^{14}N [cm^{-1}] (meas.)	^{15}N [cm^{-1}] (meas.)	^{14}N [cm^{-1}] (calcd.)	^{15}N [cm^{-1}] (calcd.)	^{14}N [cm^{-1}] (meas.)
$\nu(NH_2)$ symm.	3238 (IR)	3230 (IR)	3461	3458	3244
$\nu(NH_2)$ antisymm.	3301 (IR)	3289 (IR)	3629	3618	not resolved
ν(N–N)	1410 (IR)	masked	1442	1397	not resolved
ν(M–N)	616 (R)	596 (R)	628	613	not resolved

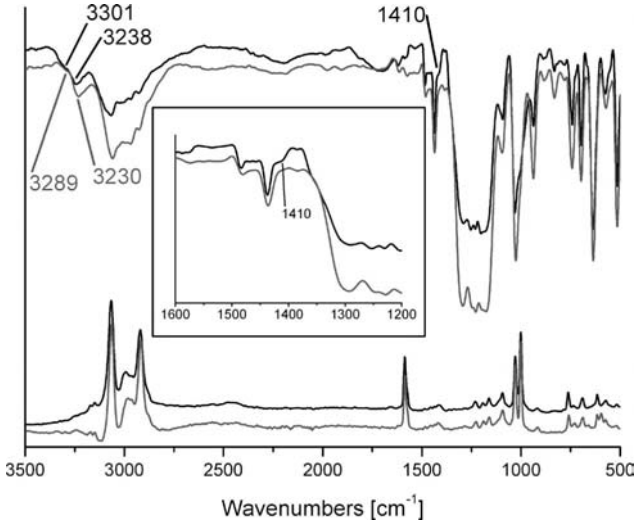

Figure 10. IR (top) and Raman (bottom) spectra of $[Mo(NNH_2)(tdppme)(dmpm)](OTf)_2$ (**4**) (black) and $[Mo(^{15}N^{15}NH_2)(tdppme)(dmpm)](OTf)_2$ (**4a**) (grey).

Raman spectra of the NNH_2 complexes **4** and **4a** show several isotope sensitive peaks in the 850 to 450 cm^{-1} region (Figure S4). In particular, a new vibration appears at 596 cm^{-1} in the spectrum of **4a** as compared to the spectrum of **4**, which is attributed to the ^{15}N-shifted Mo–N stretch. This feature appears to be at somewhat higher energy than those observed in Mo– and W–NNH_2 complexes with anionic *trans* ligands.[34]

DFT Investigations

Figure 11 shows the highest occupied (HOMO) and lowest unoccupied molecular orbitals (LUMO) of **2** and **3**. These schemes conform to the prototypical MO scheme determined for *fac*-$[Mo(N_2)(PH_3)_5]$ by Stephan et al.[22] The two LUMOs consist of the antibonding π* orbitals of the dinitrogen ligand, which lie energetically close to each other. Three energetically closely spaced MOs lie beneath. In **2** and **3** the nonbonding d_{xy} orbital of molybdenum is the highest occupied molecular orbital (HOMO). The backbonding d_{xz}–π^*_x and d_{yz}–π^*_y orbitals between molybdenum and nitrogen follow close by. The ligand orbitals lie below these; their positions and number differ because of the different substituents on the diphos ligands. The metal–ligand antibonding orbitals could only be identified if the alkyl/aryl substituents on the phosphane ligands were exchanged with hydrogen atoms. Importantly, all orbitals of **2** are shifted to higher energy with respect to those of **3** because of the lower effective nuclear charge of the Mo^0 centre in **2** than that in **3**. This conforms to the higher activation of N_2 encountered in **2** than in **3**.

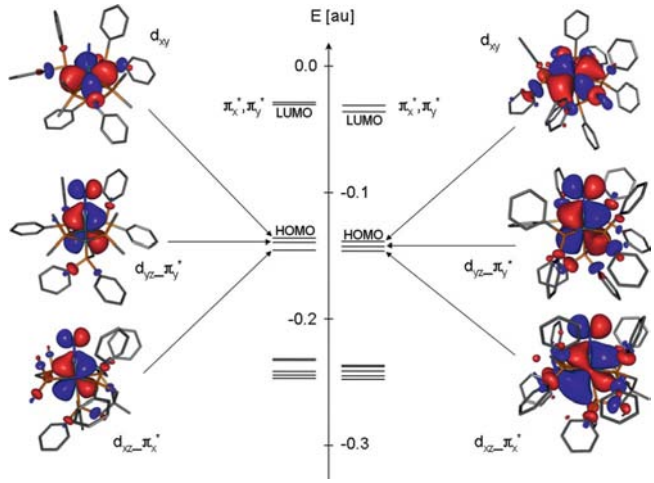

Figure 11. MO schemes of $[Mo(dmpm)(tdppme)N_2]$ (**2**) (left) and $[Mo(dppm)(tdppme)N_2]$ (**3**) (right) and representation of the three doubly occupied metal-type orbitals.

Conclusion

We were able to synthesize the first molybdenum dinitrogen complexes facially coordinated by a tripodal ligand, $[Mo(N_2)(tdppme)(dmpm)]$ (**2**) and $[Mo(N_2)(tdppme)(dppm)]$ (**3**), by sodium amalgam reduction of the molybdenum(III) precursor $[MoBr_3(tdppme)]$ (**1**) under N_2 in the presence of dppm and dppm, respectively. Compound **1** was prepared in high yield and purity from $[MoBr_3(THF)_3]$. NMR, IR and Raman spectroscopy provided valuable spectroscopic information with regard to the pentaphosphane coordination and the activation of the N_2 ligands in **2** and **3**. In the dppm complex **3**, the dinitrogen ligand is not activated for protonation. Nevertheless, it is remarkable that this complex tolerates ten phenyl groups on the coordinating phosphorus atoms. The space-filling structure derived by DFT calculations shows the impressive steric crowding around the molybdenum–N_2 moiety.

In order to increase the N_2 activation, we exchanged the dppm ligand of **3** with dmpm, which led to $[Mo(N_2)(tdppme)(dmpm)]$ (**2**). IR and Raman spectroscopy indicate a moderate activation of the N_2 ligand. The structure of this complex was investigated by X-ray crystallogra-

phy and NMR spectroscopy. The facial coordination of the tripodal ligand to the metal centre potentially resolves a fundamental problem of the Chatt cycle: the ligand exchange in *trans* position to the dinitrogen ligand. In fact, protonation of **2** with triflic acid led to the NNH_2 complex $[Mo(NNH_2)(tdppme)(dmpm)](OTf)_2$ (**4**) with retention of the pentaphosphane coordination. The NNH_2 complex **4** was again characterized by vibrational and NMR spectroscopy, coupled with DFT.

Complexes in pentaphosphane environments similar to **2** and **3**, i.e. exhibiting the combination of a tripodal and a diphos ligand, are known for other metals such as ruthenium, chromium, rhodium and cobalt.[35,36] Dinitrogen complexes containing a combination of tripodal and diphos ligands are, however, unknown to date. In the ruthenium(II) complex [RuCl(tdppme)(dmpm)], the bidentate phosphane ligand dmpm, which is less bulky than its diphenylphosphane-substituted counterpart dppm, has been chosen as a partner for the tripodal ligand tdppme.[35] The pentaphosphane coordination sphere in the chromium and rhodium complexes consists of the sterically less-demanding tripodal ligand 1,1,1-tris(dimethylphosphanylmethyl)ethane (tdmpme) and the bidentate phosphane ligand dmpm. The capability of **3** to accommodate ten phenyl groups bound to the coordinating phosphorus atoms can be attributed to the larger size of the molybdenum(0) central atom in comparison to ruthenium, chromium and rhodium centres.

The lower activation of the dinitrogen ligand in **3** in comparison to the literature-known complex $[Mo(N_2)(dpepp)(dppm)]$ can be explained by the fact that, in **3**, a diphenylphosphane donor atom is bound *trans* to the dinitrogen ligand. In contrast, in $[Mo(N_2)(dpepp)(dppm)]$, the central P atom in the dpepp ligand is coordinated *trans* to the N_2 ligand. This P atom binds two alkyl groups and one phenyl substituent, which results in a stronger activation. In complex **2**, the weaker activating potential of the tdppme tripod is compensated by the use of the bidentate alkylphosphane ligand dmpm, which allows protonation to the corresponding hydrazido complex **4**. Detailed studies investigating the possible catalytic activity of **2** in a nitrogen-fixing cycle are in progress.

Experimental Section

General: Schematic structures of the complexes prepared and investigated in this study are given in Scheme 1.

Synthesis and Sample Preparation: All reactions were carried out under a N_2 atmosphere using Schlenk techniques. All solvents were dried and freshly distilled under argon. The other reagents were used in the best available qualities. The phosphane ligands were obtained from Strem Chemicals or Sigma–Aldrich. $^{15}N_2$ (98 atom-% ^{15}N) was obtained from Sigma–Aldrich. The preparation of $[MoBr_3(THF)_3]$ was performed according to the literature.[26,27]

$[MoBr_3(tdppme)]$ (1): 1,1,1-Tris(diphenylphosphanylmethyl)ethane (500 mg, 0.800 mmol) and $[MoBr_3(THF)_3]$ (442 mg, 0.800 mmol) were heated to reflux in toluene (20 mL) for 3 h. The resulting yellow powder was washed twice with toluene (5 mL) and dried in vacuo. Yield: 736 mg (0.768 mmol, 96%). $C_{41}H_{39}Br_3MoP_3$ (960.33): calcd. C 51.28, H 4.09, Br 24.96; found C 51.14, H 4.08, Br 24.87.

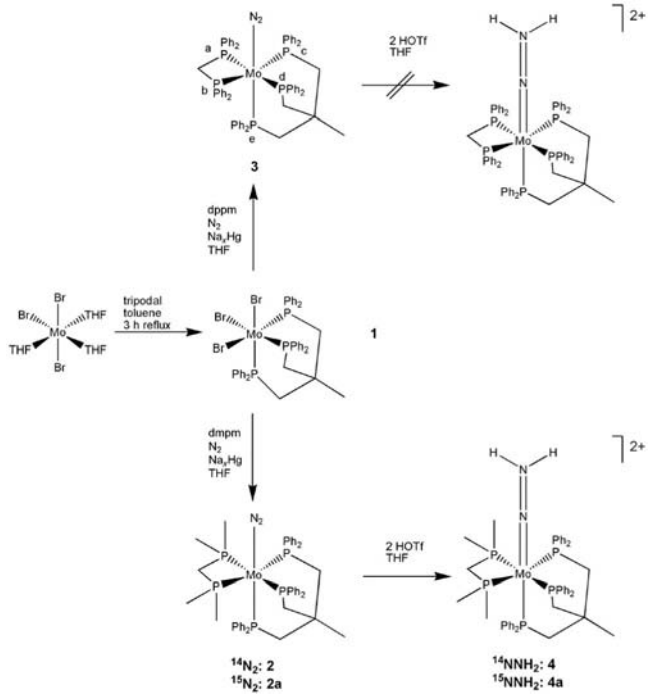

Scheme 1. Conversion of $[MoBr_3(THF)_3]$ to $[MoBr_3(tdppme)]$ (**1**) and to $[Mo(N_2)(tdppme)(dmpm)]$ (**2** and **2a**), respectively, and conversion of **1** to $[Mo(N_2)(tdppme)(dppm)]$ (**3**). Protonation of **2** and **2a** to $[Mo(NNH_2)(tdppme)(dmpm)](OTf)_2$ (**4** and **4a**). Labelling of the phosphanes is shown for **3**.

$[Mo(N_2)(tdppme)(dmpm)]$ (2) and $[Mo(^{15}N_2)(tdppme)(dmpm)]$ (2a): A suspension of **1** (500 mg, 0.52 mmol) and dmpm (71 mg, 0.52 mmol) in THF (20 mL) was added to sodium amalgam (200 mg Na, 30.0 g Hg) and stirred under nitrogen for 3 h at 0 °C and overnight at ambient temperature to obtain **2**. For the preparation of **2a**, the reaction was carried out under a $^{15}N_2$ atmosphere. The solution was decanted, filtered and reduced in vacuo to 6 mL. Methanol (6 mL) was added, and the volume of the solution was reduced again. After another addition of methanol (6 mL), a precipitate formed, which was collected by filtration, washed four times with methanol (4 mL) and dried in vacuo. Yield of **2**: 286 mg (0.323 mmol, 62%). Yield of **2a**: 304 mg (0.343 mmol, 66%). $C_{46}H_{53}MoN_2P_5$ (884.75): calcd. C 62.45, H 6.04, N 3.17; found C 62.39, H 5.86, N 2.97. $C_{46}H_{53}Mo^{15}N_2P_5$ (2227.91): calcd. C 62.31, H 6.02, N 3.38; found C 62.22, H 6.12, N 3.26. $^{31}P\{^1H\}$ CPD} NMR (161.975 MHz, C_6D_6): δ = 40.48–40.08 (m, P_e), 39.90–39.07 (m, $P_{c/d}$), –22.54 to –23.54 (m, $P_{a/b}$) ppm. $^{15}N\{^1H, ^{31}P$ CPD} NMR (40.540 MHz, C_6D_6): δ = –25.61 (d, $^1J_{NN}$ = 5.77 Hz, N_β), –33.09 to –33.63 (m, N_α) ppm. Single crystals of **2** suitable for X-ray structure determination were grown by recrystallization from a toluene/*n*-hexane mixture.

$[Mo(N_2)(tdppme)(dppm)]$ (3): A suspension of **1** (500 mg, 0.52 mmol) and dppm (200 mg, 0.52 mmol) in THF (20 mL) was added to sodium amalgam (200 mg Na, 30.0 g Hg) and stirred under nitrogen for 3 h at 0 °C and overnight at ambient temperature. The solution was decanted, filtered and reduced in vacuo to 6 mL. Methanol (6 mL) was added, and the volume of the solution was reduced again. After another addition of methanol (6 mL), a precipitate formed, which was collected by filtration, washed four

times with methanol (4 mL) and dried in vacuo. Yield: 342 mg (0.302 mmol, 58%). $C_{66}H_{61}MoN_2P_5$ (1133.03): calcd. C 69.96, H 5.43, N 2.47; found C 69.93, H 5.50, N 2.36. $^{31}P\{^1H$ CPD$\}$ NMR (161.975 MHz, C_6D_6): δ = 43.92 (dddd, $^2J_{cd}$ = –32.70, $^2J_{ac/bd}$ = –27.78, $^2J_{cb/da}$ = 91.13 Hz; $P_{c/d}$), 33.32 (ddd, $^2J_{ea/eb}$ = –22.0, $^2J_{ed/ec}$ = –24.20 Hz; P_e), 10.58 (dddd, $^2J_{ab}$ = –11.30 Hz, $P_{a/b}$) ppm.

$[Mo(NNH_2)(tdppme)(dmpm)](OTf)_2$ (4) and $[Mo(^{15}N^{15}NH_2)(tdppme)(dmpm)](OTf)_2$ (4a): Complex **2** (200 mg, 0.226 mmol) – or **2a** for the preparation of **4a** – was dissolved in THF (7 mL) and cooled to –78 °C. Triflic acid (0.04 mL, 0.443 mmol) was added. After 15 min of stirring, the solution was allowed to stand for 2 h at –78 °C and then warmed up to room temperature. *n*-Hexane (3 mL) was added, and the yellow precipitate was collected by filtration, washed three times with *n*-hexane (2 mL) and dried in vacuo. Yield of **4**: 137 mg (0.115 mmol, 51%). Yield of **4a**: 145 mg (0.122 mmol, 54%). $C_{48}H_{55}F_6MoN_2O_6P_5S_2$ (1184.89): calcd. C 48.66, H 4.68, N 2.36, S 5.41; found C 48.52, H 4.71, N 1.9, S 5.51. $C_{48}H_{55}F_6Mo^{15}N_2O_6P_5S_2$ (2528.05): calcd. C 48.57, H 4.67, N 2.53, S 5.40; found C 49.02, H 4.73, N 2.24, S 5.44. $^{31}P\{^1H$ CPD$\}$ NMR (161.975 MHz, C_6D_6): δ = 21.05 (dddd, $^2J_{cd}$ = –18.85, $^2J_{ac/bd}$ = –24.85, $^2J_{cb/da}$ = 83.15 Hz; $P_{c/d}$), –4.38 (ddd, $^2J_{ea/eb}$ = –31.03, $^2J_{ed/ec}$ = –29.44 Hz; P_e), –27.44 (dddd, $^2J_{ab}$ = –9.55 Hz, $P_{a/b}$) ppm.

Analytical Methods

Spectroscopic Characterization: Infrared spectra of the solid compounds were obtained from KBr pellets by using a Bruker IFS v66/S FTIR spectrometer. The FT-Raman spectra were recorded with a Bruker IFS 666/CS NIR FT-Raman spectrometer. A NdYAG-laser with an excitation wavelength of 1064 nm was used as a light source. The samples that absorbed at this wavelength were measured at reduced laser intensity (15%). Far-IR spectra of the solid compounds were obtained from polyethylene pellets by using a Bruker IFS 66 FIR spectrometer.

NMR spectra were recorded with a Bruker AVANCE 400 Pulse Fourier Transform spectrometer operating at frequencies of 400.13 (^1H), 161.98 (^{31}P) and 40.54 MHz (^{15}N), by using a 5-mm inverse triple-resonance probe head with *z*-gradient. Referencing was performed with tetramethylsilane ($\delta_{^1H}$ = 0 ppm), 85% H_3PO_4 ($\delta_{^{31}P}$ = 0 ppm) and neat nitromethane ($\delta_{^{15}N}$ = 0 ppm) serving as substitutive standards. All samples were measured in $[D_6]$benzene at 300 K. Spectral simulations were performed by using the MESTREC program package.

Elemental analyses were performed by using a Euro Vector CHNS-O-element analyzer (Euro EA 3000). Samples were burned in sealed tin containers in a stream of oxygen.

X-ray Structure Analysis: Intensity data were collected by using a STOE Image Plate Diffraction System with Mo-K_α radiation. The structure was solved with direct methods by using SHELXS-97. Refinement was performed against F^2 with SHELXS-97. All non-hydrogen atoms were refined anisotropically. The C–H H atoms were positioned with idealized geometry and were refined by using a riding model. A numerical absorption correction was performed (min./max. transmission: 0.7488/0.9391). The absolute structure was determined and is in agreement with the selected setting [Flack *x*-parameter: –0.08(4)].

CCDC-827075 (for **2**) contains the supplementary crystallographic data for this paper. These data can be obtained free of charge from The Cambridge Crystallographic Data Centre via www.ccdc.cam.ac.uk/data_request/cif.

Computational Details: Spin-restricted DFT calculations were performed with the B3LYP functional as implemented in Gaussian and the LANL2DZ basis set for molybdenum and 6-311G for all other elements.[28] Geometrical optimization and frequency calculations were performed with very tight thresholds in the self-consistent field (SCF) and optimization steps.

Supporting Information (see footnote on the first page of this article): $^{31}P\{1H$ CPD$\}$ and $^1H^{31}P$-HMBC NMR, Far-IR and Raman spectra are provided for some compounds.

Acknowledgments

Support by the State of Schleswig-Holstein for this research is gratefully acknowledged.

[1] O. Einsle, F. A. Tezcan, S. L. Andrade, B. Schmid, M. Yoshida, J. B. Howard, D. C. Rees, *Science* **2002**, *297*, 1696–1700.
[2] B. Schmid, M. W. Ribbe, O. Einsle, M. Yoshida, L. M. Thomas, D. R. Dean, D. C. Rees, B. K. Burgess, *Science* **2002**, *296*, 352–356.
[3] R. Y. Igarashi, M. Laryukhin, P. C. Dos Santos, H. I. Lee, D. R. Dean, L. C. Seefeldt, B. M. Hoffman, *J. Am. Chem. Soc.* **2005**, *127*, 6231–6241.
[4] B. M. Barney, T. C. Yang, R. Y. Igarashi, P. C. Dos Santos, M. Laryukhin, H. I. Lee, B. M. Hoffman, D. R. Dean, L. C. Seefeldt, *J. Am. Chem. Soc.* **2005**, *127*, 14960–14961.
[5] M. M. Georgiadis, H. Komiya, P. Chakrabarti, D. Woo, J. J. Kornuc, D. C. Rees, *Science* **1992**, *257*, 1653–1659.
[6] J. S. Kim, D. C. Rees, *Science* **1992**, *257*, 1677–1682.
[7] B. A. MacKay, M. D. Fryzuk, *Chem. Rev.* **2004**, *104*, 385–401.
[8] C. J. Pickett, *J. Biol. Inorg. Chem.* **1996**, *1*, 601–606.
[9] F. Studt, F. Tuczek, *J. Comput. Chem.* **2006**, *27*, 1278–1291.
[10] F. Studt, F. Tuczek, *Angew. Chem. Int. Ed.* **2005**, *44*, 5639–5642.
[11] D. V. Yandulov, R. R. Schrock, A. L. Rheingold, C. Ceccarelli, W. M. Davis, *Inorg. Chem.* **2003**, *42*, 796–813.
[12] D. V. Yandulov, R. R. Schrock, *Science* **2003**, *301*, 76–78.
[13] D. V. Yandulov, R. R. Schrock, *Inorg. Chem.* **2005**, *44*, 1103–1117.
[14] J. Chatt, A. J. Pearman, R. L. Richards, *Nature* **1975**, *253*, 39–40.
[15] C. J. Pickett, J. Talarmin, *Nature* **1985**, *317*, 652–653.
[16] K. Arashiba, Y. Miyake, Y. Nishibayashi, *Nat. Chem.* **2011**, *3*, 120–125.
[17] R. R. Schrock, *Nat. Chem.* **2011**, *3*, 95–96.
[18] A. Dreher, G. Stephan, F. Tuczek, *Adv. Inorg. Chem.* **2009**, *61*, 367–405.
[19] T. A. George, M. A. Jackson, B. B. Kaul, *Polyhedron* **1991**, *10*, 467–470.
[20] T. A. George, H. H. Hammund, *J. Organomet. Chem.* **1995**, *503*, C1–C3.
[21] T. A. George, M. A. Jackson, *Inorg. Chem.* **1988**, *27*, 924–926.
[22] G. C. Stephan, G. Peters, N. Lehnert, C. M. Habeck, C. Nather, F. Tuczek, *Can. J. Chem.* **2005**, *83*, 385–402.
[23] K. Klatt, G. Stephan, G. Peters, F. Tuczek, *Inorg. Chem.* **2008**, *47*, 6541–6550.
[24] G. Stephan, F. Tuczek "Synthetic Nitrogen Fixation with Transition-Metal Phosphine Complexes: New Developments" in *Activating Unreactive Substrates* (Eds.: C. Bolm, E. Hahn), Wiley-VCH, Weinheim, **2009**.
[25] T. A. George, R. C. Tisdale, *J. Am. Chem. Soc.* **1985**, *107*, 5157–5159.
[26] J. R. Dilworth, R. L. Richards, *Inorg. Synth.* **1980**, *20*, 119.
[27] C. J. H. Jacobsen, J. Villadsen, H. Weihe, *Inorg. Chem.* **1993**, *32*, 5396–5397.
[28] M. J. Frisch, G. W. Trucks, H. B. Schlegel, G. E. Scuseria, M. A. Robb, J. R. Cheeseman, G. Scalmani, V. Barone, B. Mennucci, G. A. Petersson, H. Nakatsuji, M. Caricato, X. Li, H. P. Hratchian, A. F. Izmaylov, J. Bloino, G. Zheng, J. L. Sonnenberg, M. Hada, M. Ehara, K. Toyota, R. Fukuda, J. Hase-

gawa, M. Ishida, T. Nakajima, Y. Honda, O. Kitao, H. Nakai, T. Vreven, J. J. A. Montgomery, J. E. Peralta, F. Ogliaro, M. Bearpark, J. J. Heyd, E. Brothers, K. N. Kudin, V. N. Staroverov, R. Kobayashi, J. Normand, K. Raghavachari, A. Rendell, J. C. Burant, S. S. Iyengar, J. Tomasi, M. Cossi, N. Rega, N. J. Millam, M. Klene, J. E. Knox, J. B. Cross, V. Bakken, C. Adamo, J. Jaramillo, R. Gomperts, R. E. Stratmann, O. Yazyev, A. J. Austin, R. Cammi, C. Pomelli, J. W. Ochterski, R. L. Martin, K. Morokuma, V. G. Zakrzewski, G. A. Voth, P. Salvador, J. J. Dannenberg, S. Dapprich, A. D. Daniels, Ö. Farkas, J. B. Foresman, J. V. Ortiz, J. Cioslowski, D. J. Fox, *Gaussian 09, Revision A.1* **2009**, Gaussian, Inc., Wallingford CT.

[29] S. Dilsky, *J. Organomet. Chem.* **2007**, *692*, 2887–2896.

[30] O. Walter, T. Klein, G. Huttner, L. Zsolnai, *J. Organomet. Chem.* **1993**, *458*, 63–81.

[31] T. A. George, L. Ma, S. N. Shailh, R. C. Tisdale, J. Zubieta, *Inorg. Chem.* **1990**, *29*, 4789–4796.

[32] F. Studt, F. Tuczek, *J. Comput. Chem.* **2006**, *27*, 1278–1291.

[33] H. Günther, *Angew. Chem. Int. Ed. Engl.* **1972**, *11*, 861–874.

[34] F. Tuczek, K. H. Horn, N. Lehnert, *Coord. Chem. Rev.* **2003**, *245*, 107–120.

[35] A. B. Chaplin, P. J. Dyson, *Inorg. Chem.* **2008**, *47*, 381–390.

[36] T. Suzuki, T. Tsukuda, M. Kiki, S. Kaizaki, K. Isobe, H. D. Takagi, K. Kashiwabara, *Inorg. Chim. Acta* **2005**, *358*, 2501–2512.

Received: June 23, 2011
Published Online: August 23, 2011

